ELSEVIER

PII: S0032-3861(97)10139-2

Polymer Vol. 39 No. 19, pp. 4639–4648, 1998

0032-3861/98/$19.00+0.00

Weakly segregated block copolymers: anisotropic fluctuations and kinetics of order–order and order–disorder transitions

Shuyan Qi[a] and Zhen-Gang Wang[b,*]
[a]*Division of Physics, Mathematics and Astronomy, California Institute of Technology, Pasadena, CA 91125, USA*
[b]*Division of Chemistry and Chemical Engineering, California Institute of Technology, Pasadena, CA 91125, USA*
(Received 24 June 1997; revised 2 September 1997; accepted 2 September 1997)

We discuss the kinetics of order–order and order–disorder transitions in weakly segregated diblock copolymers. A theory is developed based on the anisotropic fluctuations in the ordered phases. These fluctuations play two crucial roles: first, they determine the stability limit of the initial structure and, second, they are responsible for the emergence of new structures, whether these are the final equilibrium states or transient states during the transition. A linear stability analysis allows us to identify the largest fluctuation modes under both equilibrium and nonequilibrium conditions. By combining the order parameter of the initial structure with the largest fluctuation modes into a simplified multimode model we are able to describe qualitatively the full nonlinear evolution of the system after sudden temperature jumps beyond the spinodal of the initial phase. Our theory successfully explains our earlier results from direct Cahn–Hilliard-type numerical simulations. Our predicted kinetic scenarios are in accord with available experiments.

(Keywords: block copolymers; phase transition kinetics; anisotropic fluctuations)

1. INTRODUCTION

Dynamics of phase transitions is one of the outstanding problems in statistical physics. The most well-known and widely studied example is that of demixing (spinodal decomposition) in a binary solution or alloy upon a sudden temperature change below the spinodal line in the phase diagram. There the issues of interest are the domain growth dynamics, characterized by both the morphology of the domains and their sizes. It is well known, for example, that the domain growth dynamics in the late-stage spinodal decomposition follows a dynamic scaling, characterized by a growth exponent[1].

The dynamics of phase transitions in self-assembling complex fluids is considerably richer than spinodal decomposition in simple binary liquids or alloys and is yet relatively unexplored. Block copolymers, because of the softness of interactions and long relaxation times associated with the relevant structural changes, offer some unique opportunities for experimentally studying the pathways of phase transitions in these systems.

One of the most fascinating properties of block copolymers is their ability to self-assemble into a variety of ordered microstructures. The simplest block copolymer system is an undiluted diblock copolymer with two incompatible blocks where, upon decreasing the temperature and/or increasing the molecular weight, a variety of ordered microstructures, such as body-centre-cubic (BCC) spheres, hexagonally ordered cylinders (HEX), lamellae (LAM), and a bicontinuous gyroid (G) structure have been obtained. The equilibrium morphological behaviours of such simple diblock copolymers are now well understood[2,3].

* To whom correspondence should be addressed

In this paper, we address questions concerning the kinetics of various order–order and order–disorder transitions in weakly segregated diblock copolymers. Specifically, how does the system transform from one microstructure to another after a sudden temperature change? (This question is a valid one because in the weak segregation limit, phase transitions can be effected by changing the temperature (see *Figure 1*).) Are there interesting intermediate states during the transition? If so, what is the nature of these intermediate states? Apart from the fundamental interests, a thorough study and understanding of the kinetic pathways in phase transitions of ordered block copolymer phases may help in designing suitable processing routes for obtaining ordered structures for nanotechnology applications.

Recently, we have studied the kinetics of several order–order and order–disorder transitions after sudden temperature jumps in weakly segregated diblock copolymers using a time-dependent Ginzburg–Landau (TDGL) approach (also called the Cahn–Hilliard approach by other authors)[4,5]. Direct numerical simulation of the TDGL equations shows that, depending on the extent of the temperature jumps, these transitions often occur in several stages and can involve nontrivial intermediate states. For example, we find that melting of the hexagonal cylinder phase can involve the transient appearance of density modulations along the cylinders for small temperature jumps (which are nevertheless beyond the spinodal of the initial cylinder phase). Transition from the lamellar phase to the hexagonal cylinder phase goes through a perforated lamellar state within a certain temperature range. Our numerical findings are elucidated by a multimode analysis under the single wave number approximation. The

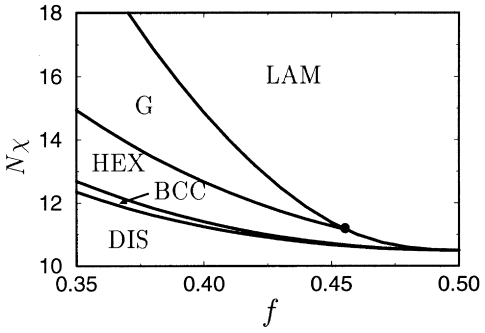

Figure 1 The meanfield phase diagram for a conformationally symmetric diblock copolymer system, calculated using the free energy equation (2)

analysis reveals that the geometric characteristics of the free energy surface, particularly saddle points and ridgelike features, are responsible for the nontrivial intermediate states on the kinetic pathways. On the basis of this analysis, a generalized kinetic 'phase diagram' is constructed, which is able to account for the different scenarios observed in the numerical simulation.

Our analysis in Refs [4,5], while essentially correct, is based on simple symmetry arguments and physical intuition. Recently, Laradji *et al*.[6], using an RPA theory of anisotropic fluctuations developed by this group of researchers[7], have addressed the stability of ordered phases. By expanding the free energy around the exact meanfield solutions to second order, these authors examined the anisotropic fluctuation in the various ordered phases. The most unstable fluctuation modes are used to infer the kinetic pathways of the order–order transitions. While it is true that the most unstable modes in an ordered phase are closely related to the transition kinetics, this information is inadequate to determine the actual pathways of the transitions for two reasons: first, the stability analysis by Laradji *et al*. is a linear one and can only predict the fastest growing modes when an ordered structure reaches its spinodal, but cannot predict the subsequent evolution of the system. Secondly, and more importantly, their stability analysis is on a stationary structure where the first derivatives of the free energy vanish, but usually the various order–order and order–disorder transitions are caused by large deviations from equilibrium conditions which result in a large deterministic driving force given by nonvanishing first derivatives of the free energy. This is important, for example, for explaining why hexagonal cylinders melt uniformly for large temperature jumps but proceed through a BCC-modulated hexagonal cylinder state when the temperature jump is small[4,5].

In this paper, we summarize our most recent efforts in understanding the kinetics of order–order and order–disorder transitions. A unified framework is developed based on anisotropic fluctuations in the ordered phases. These fluctuations are shown to play two crucial roles: first, they determine the stability limit of the initial structure and, second, they are responsible for the emergence of new structures, whether these are the final equilibrium states or transient states during the transition. A linear stability analysis allows us to identify the largest fluctuation modes under both equilibrium and nonequilibrium conditions. By combining the order parameter of the initial structure with the largest fluctuation modes into a simplified multimode model, we are able to describe qualitatively the full nonlinear evolution of the system after sudden temperature jumps beyond the spinodal of the initial phase.

This paper is organized as follows. In the next section, we discuss anisotropic fluctuations in a stationary ordered phase. This study allows us to obtain the fluctuation spectrum from which we can identify the least stable modes. The vanishing of the eigenvalue associated with the least stable modes signals the limit of stability of the structure. A key result in this section is that the least stable modes are generally located on reciprocal lattice positions that are different from those constituting the initial ordered structure. This is the very reason for the emergence of new structures. In Section 3, we discuss the kinetics of order–order and order–disorder transitions under nonequilibrium conditions. First, we perform a linear stability analysis on the dynamic equation. A key step here is the separation of the free energy driving force into a meanfield, deterministic part and a fluctuating part. The deterministic contribution serves primarily to change the amplitudes of the density waves of the initial ordered phase. The fluctuating part determines the stability of the meanfield trajectory, the deviation from which leads to the emergence of new structures. The most unstable modes give the directions of deviation from the meanfield path. Evolution beyond the linear regime is then studied by focusing on these most unstable modes together with the meanfield order parameter associated with the initial structure. This procedure provides the justification for the multimode analysis used in our earlier work. Combining the linear stability analysis with the simplified multimode analysis, we arrive at a fairly complete picture of the various kinetic scenarios. Two transitions, the lamellar (LAM) to hexagonal cylinder (HEX) transition, and the hexagonal (HEX) to disorder (DIS) transition, are used as concrete examples to illustrate the theoretical concepts. Section 4 is a summary of our main results, together with discussions of relevant experiments, and some future issues.

2. ANISOTROPIC FLUCTUATIONS AND STABILITY OF ORDERED PHASES

In this section, we discuss anisotropic fluctuations in a stationary ordered structure. The purpose of this section is two-fold: first, the analysis allows us to identify the high temperature spinodal and the largest fluctuation modes in an ordered structure; and second, and more relevant to the transition kinetics, the method of analysis can be easily extended to nonequilibrium conditions.

At a stationary state (stable, metastable, or state corresponding to a saddle point on the free energy surface), the first derivatives of the free energy with respect to the order parameters (to be specified later) vanish. The stability of the structure is determined by the matrix of the second derivatives. A stable structure, either locally or globally, is characterized by the positive definiteness of the matrix of the second derivatives. The system reaches its spinodal when the lowest eigenvalue of the matrix of the second derivatives vanishes.

The stability of a structure is intimately related to the spontaneous, thermal fluctuations in that structure. A structure is stable if the mean-square fluctuations of the order parameter are finite, and becomes unstable when any mean-square fluctuations diverge. In an ordered diblock copolymer phase, the fluctuations are generally anisotropic because of the anisotropy of the ordered structure. The structure reaches its spinodal when the largest fluctuation becomes divergent. These largest, or most unstable,

modes dictate the potential direction for the spontaneous emergence of new structures.

A rigorous approach for studying anisotropic fluctuations based on the exact self-consistent solutions has been developed by Shi and co-workers[7]. Here, we provide a simpler, approximate approach based on an order-parameter free energy functional. Although not accurate enough for quantitative purposes, the current approach is simpler to implement and is mathematically more transparent than the rigorous one. The order parameter approach is also more suitable for studying kinetics. Since the issues addressed in this paper do not depend on quantitative accuracy, we choose this simpler approach.

We start with the standard Leibler free energy functional[8] for incompressible diblock copolymers:

$$F[\psi(\vec{k})] = \frac{1}{2}\int d\vec{k}\Gamma_2(\vec{k}, -\vec{k})\psi(\vec{k})\psi(-\vec{k}) + \frac{1}{3!}\int d(\vec{k}_1\vec{k}_2) \times \Gamma_3(\vec{k}_1, \vec{k}_2, -\vec{k}_1-\vec{k}_2)\psi(\vec{k}_1)\psi(\vec{k}_2)\psi(-\vec{k}_1-\vec{k}_2) + \frac{1}{4!}\int d(\vec{k}_1\vec{k}_2\vec{k}_3)\Gamma_4(\vec{k}_1, \vec{k}_2, \vec{k}_3, -\vec{k}_1-\vec{k}_2-\vec{k}_3) \times \psi(\vec{k}_1)\psi(\vec{k}_2)\psi(\vec{k}_3)\psi(-\vec{k}_1-\vec{k}_2-\vec{k}_3). \quad (1)$$

In the above equation, $\psi(\vec{k}) = \rho_A(\vec{k}) - f$ is the order parameter where $\rho_A(\vec{k})$ is the Fourier transform of the local density of A-monomers and f is the global fraction of the A-block. $\Gamma_2(\vec{k}_1, \vec{k}_2)$, $\Gamma_3(\vec{k}_1\vec{k}_2\vec{k}_3)$, and $\Gamma_4(\vec{k}_1, \vec{k}_2, \vec{k}_3, \vec{k}_4)$ are in general wavevector-dependent coefficients in the expansion (called the two-point, three-point, and four-point vertex functions, respectively, in field-theoretical jargon). The two-point vertex function has the form of $\Gamma_2(\vec{k}, -\vec{k}) = S_0^{-1}(k) - 2N\chi$, where N is the degree of polymerization, χ is the Flory–Huggins parameter, and $S_0(k)$ is the structure factor for a non-interacting diblock copolymer and is peaked at a wavenumber k^*. In the weak-segregation regime, the density waves are dominated by wavevectors with the optimal wavenumber k^*. Thus we approximate the functions $\Gamma_3(\vec{k}_1, \vec{k}_2, \vec{k}_3)$ and $\Gamma_4(\vec{k}_1, \vec{k}_2, \vec{k}_3, \vec{k}_4)$ by their values corresponding to wavevectors having the optimal magnitude k^*. In this approximation, $\Gamma_3(\vec{k}_1, \vec{k}_2, \vec{k}_3)$ becomes independent of the wavevectors while $\Gamma_4(\vec{k}_1, \vec{k}_2, \vec{k}_3, \vec{k}_4)$ has only a weak angular dependence. We further ignore the angular dependence in Γ_4 by the approximation $\Gamma_4(\vec{k}_1, \vec{k}_2, \vec{k}_3, \vec{k}_4) = \Gamma_4(0, 0)$, where $\Gamma_4(0,0)$ is a function defined in Ref. [8]. We denote these functions as γ_3 and γ_4, respectively. These approximations are not necessary and are not expected to have any significant effects on the issue we wish to address in this paper, but greatly simplify the calculations and make the results much more transparent. Thus we write the free energy functional as:

$$F[\psi(\vec{k})] = \frac{1}{2}\int d\vec{k}[S_0^{-1}(k) - 2N\chi]\psi(\vec{k})\psi(-\vec{k}) + \frac{\gamma_3}{3!}\int d(\vec{k}_1\vec{k}_2)\psi(\vec{k}_1)\psi(\vec{k}_2)\psi(-\vec{k}_1-\vec{k}_2) + \frac{\gamma_4}{4!}\int d(\vec{k}_1\vec{k}_2\vec{k}_3)\psi(\vec{k}_1)\psi(\vec{k}_2)\psi(\vec{k}_3)\psi(-\vec{k}_1-\vec{k}_2-\vec{k}_3). \quad (2)$$

$S_0^{-1}(k)$ and γ_4 can be calculated easily using standard methods[8,9]. These functions depend on the fraction f of the A-block and on the conformation asymmetry between the two blocks. For simplicity, we shall only consider conformationally symmetric diblocks in the rest of the paper, but the general approach is equally applicable to conformationally asymmetric cases.

The meanfield order parameter $\psi_0(\vec{k})$ for a given morphology can be written as:

$$\psi_0(\vec{k}) = \sum_{\vec{G}} A_{\vec{G}}\delta(\vec{k}-\vec{G}) \quad (3)$$

where $\vec{G}$ is the set of reciprocal lattice wavevectors of the morphology, and the $A_{\vec{G}}$'s are obtained by minimizing the free energy equation (2) by substituting equation (3) into the free energy.

To study the fluctuation around the meanfield structure, we write

$$\psi(\vec{k}) = \psi_0(\vec{k}) + \Delta\psi(\vec{k}). \quad (4)$$

Substituting this into equation (2), keeping terms only up to quadratic order in $\Delta\psi(\vec{k})$ and noting the stationary condition for $\psi_0(\vec{k})$, we obtain

$$F[\psi(\vec{k})] = F[\psi_0(\vec{k})] + \frac{1}{2}\int d\vec{k}[S_0^{-1}(k) - 2N\chi] \times \Delta\psi(\vec{k})\Delta\psi(-\vec{k}) + \frac{\gamma_3}{2}\sum_{\vec{G}}\int d\vec{k}A_{\vec{G}}\Delta\psi(\vec{k})\Delta\psi(-\vec{k}-\vec{G}) + \frac{\gamma_4}{4}\sum_{\vec{G}}\sum_{\vec{G}'}\int d\vec{k}A_{\vec{G}}A_{\vec{G}'}\Delta\psi(\vec{k})\Delta\psi(-\vec{k}-\vec{G}-\vec{G}'). \quad (5)$$

The presence of periodic order makes the fluctuations in $\vec{k}$-space non-diagonal. To study the anisotropic fluctuation and the stability of the ordered phases, the quadratic term of free energy needs to be diagonalized. This generally requires diagonalization of a very large matrix. In this work, we make the simplifying approximation that the dominant fluctuation arises from modes with wavevectors $|\vec{k}| \approx k^*$. This approximation is justified in the weak segregation regime where fluctuations are mainly determined by the leading quadratic coefficient $S_0^{-1}(k) - 2N\chi$ which has a minimum at $k = k^*$. Using this approximation, the matrix can be truncated to a smaller matrix involving $\vec{k}$ and $\vec{k} \pm \vec{G}$, and can then be diagonalized analytically; the eigenvalues of this matrix determine the stability of an ordered structure. The structure is stable or metastable if all the eigenvalues are positive. The spinodal of a structure is reached when the lowest eigenvalue turns negative.

The structure factor of an ordered phase when it is stable or metastable is given by

$$\langle\psi(\vec{k})\psi(-\vec{k})\rangle = \psi_0(\vec{k})\psi_0(-\vec{k}) + \langle\Delta\psi(\vec{k})\Delta\psi(-\vec{k})\rangle. \quad (6)$$

The fluctuation part of the structure factor $\langle\Delta\psi(\vec{k})\Delta\psi(-\vec{k})\rangle$ is obtained by taking the diagonal element of the inverse matrix of equation (5).

We now illustrate the theory by applying it to the lamellar and hexagonal cylinder phases.

2.1 Anisotropic fluctuations in the lamellar phase

For the meanfield lamellar structure, we assume a sinusoidal wave in the z-direction for the order parameter, with $k_z = k^*$. The amplitude of the meanfield lamellar wave is obtained by minimizing the free energy equation (2).

To study the fluctuation spectrum and the stability of the lamellar phase, we consider a small perturbation of the form given by equation (4). The diagonalization of the matrix in equation (5) can be easily performed with the result that the lowest eigenvalues lie on two rings at $k_z = \pm (1/2)k^*$

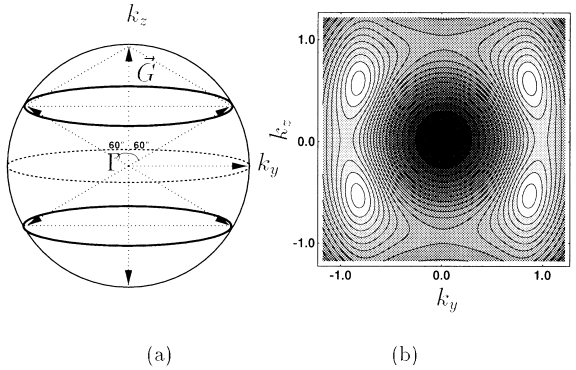

Figure 2 (a) A schematic showing the two rings in the k-space at $k_z = \pm \frac{1}{2}k^*$ corresponding to the least stable fluctuation modes in a lamellar structure of wavevector $k_z = k^*$. (b) The fluctuation part of the scattering pattern of the LAM phase with $N\chi = 18.0$ for $f = 0.35$ in $k_x = 0$ plane in units of k^*. The two Bragg spots at $k_z = \pm k^*$, $k_y = 0$ due to the meanfield lamellar wave are not shown

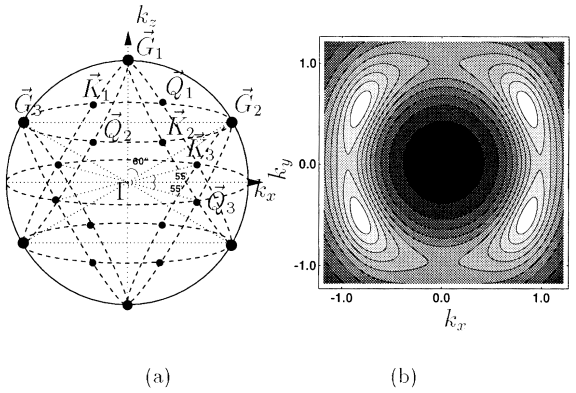

Figure 3 (a) Locations of the largest fluctuation modes of the HEX phase in k-space. The 18 spots constitute the set of the smallest wavevectors of a twinning BCC structure. (b) Calculated structure factor for the HEX phase in the $k_z = 0$ plane. The parameters are $f = 0.35$ and $N\chi = 13.0$

and $|\vec{k}| = k^*$, as shown in *Figure 2a*. Thus the dominant fluctuations, i.e. the least stable fluctuation modes will come from wavevectors on these rings.

Figure 2 shows the fluctuation contribution to the structure factor in the $k_x = 0$ plane of the LAM phase with $f = 0.35$ in the metastable state near the spinodal. The scattering due to fluctuations at

$$k_z = \pm \tfrac{1}{2}k^* \quad \text{and} \quad k_y = \pm \frac{\sqrt{3}}{2}k^*$$

is a result of the intersection of the rings with $k_x = 0$ plane. The same scattering pattern was obtained earlier by Yenug *et al.*[7] using a more rigorous approach.

As $N\chi$ decreases, fluctuations on the two rings in *Figure 2* will increase. The vanishing of the eigenvalue corresponding to these least stable modes, or equivalently, the divergence of the fluctuations of these modes, signals the spinodal of the lamellar phase.

Although the scattering pattern resulting from the linear stability analysis lacks any in-layer structure (in the x,y plane), the finding that the dominant fluctuations occur at

$$k_z = \pm \tfrac{1}{2}k^*$$

leads to the important conclusion that any structures that form as a result of instability of the LAM phase will have a periodicity of two layers.

The location of the largest fluctuation modes in k-space can be understood with a simple geometric argument. In the presence of a periodic structure, the fluctuations interact with the meanfield order parameter associated with the ordered structure, and become anisotropic as a result. Such interactions satisfy a momentum conservation as manifested in the forms of the last two terms in equation (5). In the weak segregation regime, the meanfield order parameter is dominated by Fourier modes with reciprocal lattice wavevectors $|\vec{G}| = k^*$. The dominant fluctuations are also from modes with wavevectors $|\vec{k}| \approx k^*$. Thus we focus on fluctuations with $|\vec{k}| = k^*$. Take the γ_3-term first. The restriction that the wavevectors of the fluctuations be on a sphere with $k = k^*$ means $|\vec{k}| = k^*$ and $|\vec{k} \pm \vec{G}| = k^*$. Since $|\vec{G}| = k^*$, it follows that the dominant fluctuations, as a result of interacting with the meanfield order parameter with a wavevector $\vec{G}$, are on the ring formed by the intersection between the sphere $|\vec{k}| = k^*$ and the plane $\vec{k} = \pm (1/2)\vec{G}$. A similar analysis of the γ_4-term yields two types of contributions: an isotropic contribution when $\vec{G}' = -\vec{G}$ and an anisotropic contribution when $\vec{G} + \vec{G}' = \vec{G}''$ where $\vec{G}'$ and $\vec{G}''$ are other reciprocal lattice wavevectors. For the lamellar phase in the weak segregation limit, the second contribution will be small since either $\vec{G}$ or $\vec{G}'$ or $\vec{G}''$ will have to be outside the spherical shell $|\vec{k}| = k^*$. For a nonlamellar structure, e.g. for hexagonal cylinders, it is possible to satisfy $\vec{G} + \vec{G}' = \vec{G}''$ while still having $|\vec{G}| = |\vec{G}'| = |\vec{G}''| = k^*$ In that case the analysis becomes identical to that for the γ_3-term.

2.2 Anisotropic fluctuations in the hexagonal cylinder phase

The hexagonal cylinder (HEX) structure in the weak segregation limit can be represented as a superposition of six co-planar density waves with wavevectors that are 60° apart from each other. The positions of these wavevectors in k-space are indicated by the six large black dots at $\pm \vec{G}_1$, $\pm \vec{G}_2$, $\pm \vec{G}_3$ in *Figure 3*. The amplitude of the density wave is obtained by minimizing the free energy, and the fluctuation spectrum can be obtained using the method described earlier.

To locate the positions of the largest fluctuation modes in k-space, we use the simple geometric construction outlined in Section 2.1. For each of the six reciprocal lattice wavevectors we form a plane that is perpendicular to the wavevector and that cuts the wavevector by half. The intersection of this plane with the spherical shell $|\vec{k}| = k^*$ forms a ring. This construction results in six rings associated with the six reciprocal lattice wavevectors. Fluctuation modes will be larger on these rings than elsewhere, and will be the largest at points where two rings intersect. There are 18 such points, six of which coincide with the positions of the original HEX waves, and the other 12 are shown by the dots at $\pm \vec{K}_1$, $\pm \vec{K}_2$, $\pm \vec{K}_3$ and $\pm \vec{Q}_1$, $\pm \vec{Q}_2$, $\pm \vec{Q}_3$ in *Figure 3*. These 18 spots constitute the reciprocal lattice of a twinning BCC structure. Therefore, the anisotropic fluctuations in the HEX phase are on a twinning BCC structure. The twinning BCC structure was observed in the experiment by Almdal *et al.*[10] by dynamically shearing the BCC phase of a poly(ethylenepropylene)–poly(ethylethylene) diblock copolymer. Their scattering pattern agrees well with our *Figure 3b*. They interpreted the twinning BCC structure as arising from the shear deformation of the initial structure. An alternative interpretation is that shear destroys the BCC structure and turns it into the cylinder phase with large fluctuations. What they observed could be the fluctuation from the HEX phase rather than Bragg peaks from a twinning BCC structure.

The analysis in this section identifies the least stable fluctuation modes in an ordered block copolymer structure. These modes provide hints of the potential evolution of the system when the spinodal is reached. However, to address the kinetics of phase transition, we need to study the nature of anisotropic fluctuation under general non-equilibrium conditions where there is a nonvanishing thermodynamic driving force. This task is undertaken in the next section.

3. KINETICS OF ORDER–ORDER AND ORDER–DISORDER TRANSITIONS

We describe the dynamic evolution of the order parameter by a time-dependent Ginzburg–Landau equation:

$$\frac{\partial\psi(\vec{r},t)}{\partial t}=\int \mathrm{d}\vec{r}\,' M(\vec{r}-\vec{r}\,')\nabla^2_{\vec{r}\,'}\left[\frac{\delta F}{\delta\psi(\vec{r}\,')}\right]+\eta(\vec{r},t) \qquad (7)$$

where $M(\vec{r}-\vec{r}\,')$ is a mobility coefficient which is in general nonlocal[11–16] and $\eta(\vec{r},t)$ is a random fluctuating force with zero mean and with a variance satisfying the fluctuation–dissipation theorem:

$$\langle\eta(\vec{r},t)\eta(\vec{r}\,',t')\rangle=-2k_{\mathrm{B}}T\nabla^2_{\vec{r}}M(\vec{r}-\vec{r}\,')\delta(t-t'). \qquad (8)$$

It is convenient to work with the Fourier modes of the order parameter. In the Fourier representation, equation (7) becomes

$$\frac{\partial\psi(\vec{k})}{\partial t}=-k^2M(\vec{k})\left[\frac{\delta F}{\delta\psi(-\vec{k})}\right]+\eta(\vec{k},t) \qquad (9)$$

while equation (8) becomes

$$\langle\eta(\vec{k},t)\eta(\vec{k}\,',t')\rangle=2(2\pi)^3k_{\mathrm{B}}Tk^2M(\vec{k})\delta(\vec{k}+\vec{k}\,')\delta(t-t'). \qquad (10)$$

A general expression for the mobility coefficient $M(k)$ has been derived by Kumaran and Fredrickson[16]; it is:

$$M(k)=DS_0(k) \qquad (11)$$

where $S_0(k)$ is the structure factor for the same diblock copolymer in the absence of enthalpic interaction (i.e. with $N\chi=0$), and D is the diffusivity of the polymer chains whose scaling behaviour depends on whether the chains are entangled or not.

We define an effective kinetic coefficient $\lambda(\vec{k})=k^2M(\vec{k})$. In the weak segregation limit, the order parameter as well as fluctuations are dominated by wavevectors with $|\vec{k}|=k^*$ Thus it is reasonable to replace the k-dependent $\lambda(\vec{k})$ by $\lambda(k^*)$. $\lambda(\vec{k})$ also becomes independent of k in the limit of large $|\vec{k}|$. Therefore henceforth we will take $\lambda(\vec{k})$ to be a constant λ, and equation (9) simplifies to

$$\frac{\partial\psi(\vec{k})}{\partial t}=-\lambda\left[\frac{\delta F}{\delta\psi(-\vec{k})}\right]+\eta(\vec{k},t). \qquad (12)$$

Equation (10) also simplifies correspondingly.

3.1 Deterministic versus fluctuation driving forces: linear stability analysis

In equation (12), the order parameter $\psi(\vec{k})$ includes both a part that represents the structure of the initial phase and a part due to fluctuations. To gain insights and to make use of the concept of anisotropic fluctuations, it is instructive to write the order parameter as a sum of a meanfield part $\psi_0(\vec{k})$ and a fluctuating part $\Delta\psi(\vec{k})$, in the same form as in equation (4), but now allowing both $\psi_0(\vec{k})$ and $\Delta\psi(\vec{k})$ to be time-dependent. Substituting equation (4) into equation (12), we obtain, to linear order in $\Delta\psi(\vec{k})$ (to be consistent with the level of treatment of equilibrium fluctuations in the previous section):

$$\frac{\partial\psi_0(\vec{k})}{\partial t}=-\lambda\left[\frac{\delta F}{\delta\psi(-\vec{k})}\right]_0 \qquad (13)$$

and

$$\frac{\partial\Delta\psi(\vec{k})}{\partial t}=-\lambda\int \mathrm{d}\vec{k}'\left[\frac{\delta^2F}{\delta\psi(-\vec{k})\delta\psi(\vec{k}')}\right]_0\Delta\psi(\vec{k}')+\eta(\vec{k},t) \qquad (14)$$

where the subscript '0' indicates that the derivatives are taken at $\psi(\vec{k})=\psi_0(\vec{k})$. More explicitly, using equation (2) for the free energy, equation (13) and equation (14) become, respectively,

$$\frac{\partial A_{\vec{G}}}{\partial t}=-\lambda\left\{[S_0^{-1}(k^*)-2N\chi]A_{\vec{G}}+\frac{\gamma_3}{2}\sum_{\vec{G}'}A_{\vec{G}'}A_{\vec{G}-\vec{G}'}+\frac{\gamma_4}{6}\sum_{\vec{G}'}\sum_{\vec{G}''}A_{\vec{G}'}A_{\vec{G}''}A_{\vec{G}-\vec{G}'-\vec{G}''}\right\} \qquad (15)$$

and

$$\frac{\partial\Delta\psi(\vec{k})}{\partial t}=-\lambda\left\{[S_0^{-1}(k)-2N\chi]\Delta\psi(\vec{k})+\gamma_3\sum_{\vec{G}}A_{\vec{G}}\Delta\psi(\vec{k}-\vec{G})+\frac{\gamma_4}{2}\sum_{\vec{G}}\sum_{\vec{G}'}A_{\vec{G}}A_{\vec{G}'}\Delta\psi(\vec{k}-\vec{G}-\vec{G}')\right\}+\eta(\vec{k},t) \qquad (16)$$

where we have used our ansatz equation (3) for the mean-field order parameter.

The equation for the meanfield order parameter, equation (15), describes a steepest descent path along the gradient of the (meanfield) free energy. Thus, if the system finds itself in a nonequilibrium condition, as after a temperature jump, the meanfield order parameter will follow a downhill path until the gradient vanishes. It is clear from equation (15), that if we start with a structure described by the meanfield order parameters $\{A_{\vec{G}}\}$, the system will remain in that structure; only the magnitude of the order parameter changes. Thus the meanfield path corresponds to a trivial dynamics. Deviation from such trivial, meanfield dynamics is due to anisotropic fluctuations. As we showed in the last section, fluctuations in ordered structures are anisotropic and generally the largest fluctuations are located at different positions in Fourier space than the reciprocal lattice positions of the original structure. Thus the emergence of new structures on the kinetic pathway is a result of anisotropic fluctuations: these fluctuations determine whether the meanfield deterministic path is stable.

The coefficient of the linear term on the right hand side of equation (16) has the same form as that in equation (5). However, in equation (5) the meanfield order parameters are those that minimize the free energy, and are hence time independent, whereas in equation (16) the order parameters in general do not correspond to an equilibrium condition and are time dependent. This makes the analysis of equation (16) difficult. However, our main concern here is to determine the local, instantaneous stability of equation (15), for which we only need to know if a certain fluctuation around an

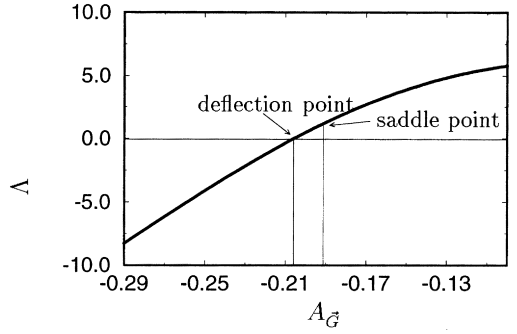

Figure 4 Growth rate of the least stable fluctuation modes Λ (in units of λ) as a function of the LAM order parameter at $f = 0.35$ and $(N\chi)_f = 15.0$. After a temperature jump, $A_{\vec{G}}$ evolves in the direction of decreasing $|A_{\vec{G}}|$. The saddle point of the LAM at this $N\chi$ value is at $A_{\vec{G}} = -0.1911$

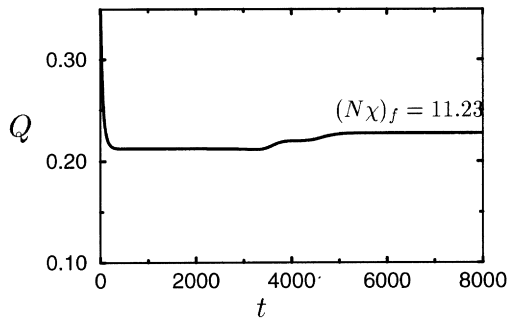

Figure 5 Temporal evolution of the global order parameter Q during the LAM to HEX transition at $f = 0.45$ for the temperature jump from $(N\chi)_i = 12.0$ to $(N\chi)_f = 11.03$

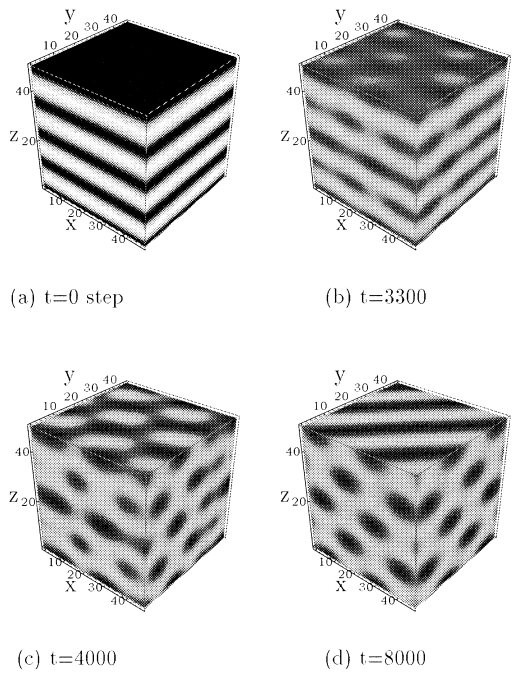

Figure 6 Microstructural evolution after a temperature jump from LAM to HEX at $f = 0.45$ ($(N\chi)_i = 12.0$, $(N\chi)_f = 11.03$); data taken at various stages of the simulation

instantaneous value of $A_{\vec{G}}$, will grow or decay. For this purpose, it suffices to analyze the growth rate matrix on the right-hand side of equation (16). This is the same matrix as the quadratic coefficient in equation (5) multiplied by -2λ, and its analysis thus can be performed following the same procedure as outlined in Section 2. In particular, the locations of the least stable fluctuation modes in k-space remain the same; but the stability of these modes now depends on the instantaneous value of $A_{\vec{G}}$. When all eigenvalues of the matrix are negative, the meanfield path is stable, and when one or more eigenvalues turn positive, the meanfield path becomes unstable, signalling the emergence of new structure. The new structure should now be represented by adding the most unstable modes to the meanfield order parameter.

We now use these theoretical ideas to discuss the kinetics of phase transitions after a sudden temperature jump, using the LAM to HEX and HEX to DIS transitions as concrete examples.

Consider the LAM to HEX transition first. We start from a well-ordered LAM structure in equilibrium at $(N\chi)_i$ in the LAM region of the phase diagram characterized by a one-dimensional sinusoidal wave with wavevector $\vec{G}$ and amplitude $A_{\vec{G}}$. Now imagine making a temperature jump, i.e., decreasing $N\chi$ to $(N\chi)_f$ in the HEX region of the phase diagram, beyond the spinodal limit of the LAM phase. Due to the deviation from equilibrium, $A_{\vec{G}}$ will evolve according to equation (15). However, even though $(N\chi)_f$ is now beyond the spinodal of the LAM phase, the initial stage of the evolution is a simple decay of the LAM order parameter, i.e. the evolution is well described by equation (15) and the fluctuations, the largest of which are located on the rings in *Figure 2*, are still stable, due to the large value of $A_{\vec{G}}$. This is shown in *Figure 4* where we plot the growth exponent of the least stable fluctuation mode as a function of the lamellar order parameter $A_{\vec{G}}$ ($A_{\vec{G}}$ is chosen to be negative to satisfy the correct phase relationship). For large, negative values of $A_{\vec{G}}$, the exponent is negative. As $A_{\vec{G}}$ decays (according to equation (15)) the deterministic driving force decreases and, at some point, the fluctuation becomes unstable, and new structures corresponding to the two rings in *Figure 2* begin to emerge. Note that the onset of the instability, i.e. deflection from the meanfield path, occurs before the system reaches a saddle point.

The above-described scenario is in agreement with the result obtained from direct numerical simulation of the Ginzburg–Landau equation*. *Figure 5* shows the simulation result for the temporal behaviour of a global order parameter defined as

$$Q = \sqrt{\sum_{\vec{r}} \psi(\vec{r})^2} = \sqrt{\sum_{\vec{k}} \psi_k \psi_{-k}}$$

for a temperature jump from $(N\chi)_i = 12.0$ to $(N\chi)_f = 11.03$. The initial rapid decrease in the order parameter as well as the plateau that follows are well described by the meanfield equation (equation (15)). Direct visual inspection of the gray level plot of the microstructure during this stage does not reveal any specific structure within the lamellar layers. Thus the system remains in the lamellar phase, with a decreased order parameter. At the end of the plateau, however, the global order parameter increases, and at the same time in-layer density undulations begin to emerge as shown in *Figure 6b*. This signals the instability of the meanfield path and the growth of the fluctuation mode. Note that the

* In the numerical simulation, we used a constant local mobility coefficient in equation (7); we also used a free energy which differs slightly from the Leibler free energy equation (2). There we focus on the qualitative rather than quantitative agreements.

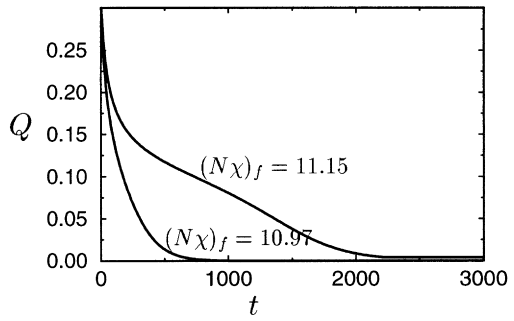

Figure 7 Evolution of the global order parameter Q for the temperature jump from the HEX to DIS phase at $f = 0.4$ with $(N\chi)_i = 11.71$

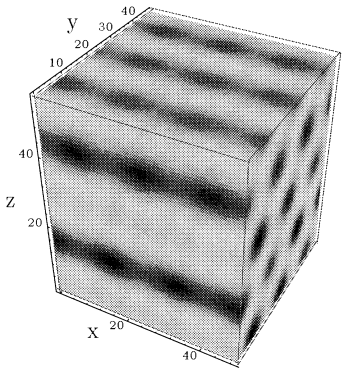

Figure 8 Intermediate state during the HEX to DIS transition at $f = 0.4$ ($(N\chi)_i = 11.71$, $(N\chi)_f = 11.15$), taken at $t = 1000$

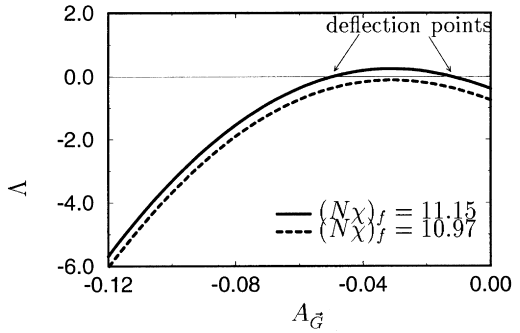

Figure 9 Growth rate of the least stable fluctuation modes Λ (in units of λ) as a function of the HEX order parameter at $f = 0.4$ for two final values of $N\chi$. After a temperature jump $A_{\vec{G}}$ evolves in the direction of decreasing $|A_{\vec{G}}|$. For the smaller temperature jump ($(N\chi)_f = 11.15$), the meanfield kinetic path becomes unstable at the first deflection point and, between the two deflection points, the free energy surface has a ridgelike feature

fluctuations have a periodicity in the z-direction of twice the lamellar spacing; this is in excellent agreement with the prediction that the most unstable modes are on the rings at

$$k_z = \pm \tfrac{1}{2} k^*$$

see *Figure 2*.

We now discuss the HEX to DIS transition, this time starting with the simulation results. *Figure 7* shows the evolution of the global order parameter for two temperature jumps. For the large temperature jump to $(N\chi)_f = 10.97$, the order parameter decays in a simple manner, suggesting direct melting of the cylinders. Gray level plots of the order parameter at various times show no structure change as the cylinder melts.

In contrast, the behaviour of Q in the case of the smaller temperature jump (to $(N\chi)_f = 11.15$) suggests a nontrivial melting process. The slower decay at intermediate times is accompanied by the formation of structures along the cylinders: the cylinders seem to first break into spheres and the melting proceeds via this modulated hexagonal cylinder (MHC) phase. This transient structure is clearest between the two inflection points on the curve, because at long times the structure has all but melted and at short times the structure is dominated by the hexagonal cylindrical structure of the initial state. *Figure 8* shows the transient MHC state.

These two qualitatively different behaviours can be understood by analyzing the stability of the meanfield equation (equation (15)). For the large temperature jump, fluctuations are stable along the entire path. On the other hand, for the smaller temperature jump, fluctuations become unstable on certain parts of the meanfield path. These two different behaviours are shown by plotting the growth rate of the least stable modes as a function of the order parameter of the HEX wave; see *Figure 9*. Since the least stable fluctuations form a twinning BCC structure (or BCC structure if we restrict to perfect periodic structures), the growth of the fluctuation modes leads to the appearance of a modulated hexagonal cylinder (MHC) structure which is the superposition of the HEX and BCC waves. A critical value of the final $N\chi$ can be located that separates these two different kinetic behaviours. The result is

$$(N\chi)_c = (N\chi)^* - 2\gamma_3^2/(5\gamma_4), \text{ where } (N\chi)^* = \tfrac{1}{2}S_0^{-1}(k^*)$$
$$(\text{for } f = 0.4,\ (N\chi)_c = 10.97)$$

For $(N\chi)_f > (N\chi)_c$, a nontrivial pathway for the HEX to DIS transition is expected, where the cylinders will first go through an MHC structure before melting; whereas if $(N\chi)_f < (N\chi)_c$, a direct featureless melting is expected. These behaviours are captured in *Figure 9*: the curve for the smaller temperature jump to $(N\chi)_f = 11.15$ has two deflection points suggesting a ridgelike structure on the free energy surface between these two points (see *Figure 13*) while the curve for the larger temperature jump to $(N\chi)_f = 10.97$ indicates that the fluctuations are stable, consistent with a simple melting of the HEX structure.

3.2 Beyond the linear regime: a simplified multimode analysis

The linear stability analysis in Section 3.1 yields information about whether the meanfield path is stable, when it becomes unstable, and if it does become unstable in which direction the system will evolve. However, further evolution of these fluctuation into a three-dimensional structure cannot be predicted by such a linear stability analysis.

In this section, we describe a simplified multimode analysis, which, although lacking in mathematical rigor, has the merit of being physically intuitive, and captures essentially all the qualitative dynamical behaviours revealed by our computer simulation studies. This analysis was first proposed by us in Refs[4,5], based on symmetry and physical intuition. Here we provide a more rigorous justification.

We have shown in Section 2 and Section 3.1, that the largest fluctuation modes of an ordered phase are located at positions in k-space usually different from those corresponding to the meanfield order parameter of the initial structure. When the meanfield kinetic path becomes unstable,

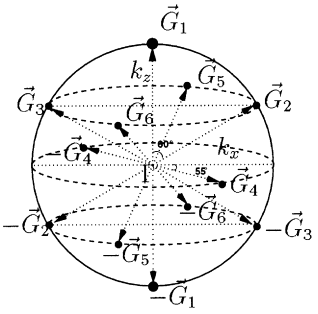

Figure 10 The 12 first-order wavevectors for a BCC structure

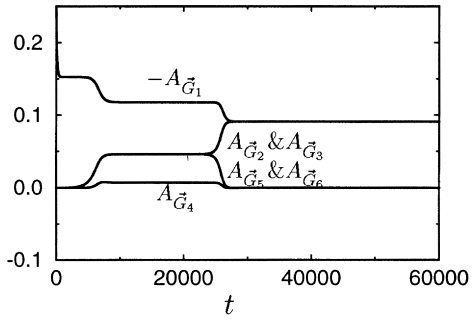

Figure 11 Evolution of the wave amplitudes during the LAM to HEX transition at $f = 0.45$ ($(N\chi)_i = 12.0$, $(N\chi)_f = 11.03$). Note the appearance of two plateaus beside the final HEX state

these fluctuation will grow and will become part of the new order parameter. This suggests that one can construct an expanded order parameter space that includes both the original order parameter and the dominant fluctuation modes. In the weak segregation limit, both the order parameter and the fluctuation are dominated by modes with $|\vec{k}| = k^*$. Thus we choose a set of waves $A_{\vec{G}}$ with wavevectors $|\vec{G}| = k^*$. If we restrict our consideration to spatially periodic structures, a minimal set of wavevectors that can represent the LAM, HEX, BCC, as well as intermediate states during the transitions are the 12 first-order reciprocal lattice wavevectors of a BCC lattice. These wavevectors are shown in *Figure 10*. The order parameter is then represented by

$$\psi(\vec{r}) = \sum_{\vec{G}} A_{\vec{G}} \exp(i\vec{G}\cdot\vec{r}) \tag{17}$$

where the $A_{\vec{G}}$ values are the amplitudes associated with the wavevectors $\vec{G}$ (we use the same notation $A_{\vec{G}}$ for both the order parameter of the initial structure and the dominant fluctuation modes). By considering only periodic structures, we may choose $A_{\vec{G}}$ to be real; then $A_{-\vec{G}} = A_{\vec{G}}$. In this construction, the LAM phase is represented by a nonzero $A_{\vec{G}_1}$ ($= A_{-\vec{G}_1}$) with all other amplitudes being zero; the HEX phase is obtained by either the wavevectors $\vec{G}_1$, $\vec{G}_2$, $\vec{G}_3$, or $\vec{G}_1$, $\vec{G}_5$, $\vec{G}_6$; the BCC phase requires all six wavevectors with equal amplitudes. Evolution of the order parameter is then described by

$$\frac{\partial A_{\vec{G}}}{\partial t} = -\lambda\left\{\left[S_0^{-1}(k^*) - 2N\chi\right]A_{\vec{G}} + \frac{\gamma_3}{2}\sum_{\vec{G}'} A_{\vec{G}'}A_{\vec{G}-\vec{G}'} + \frac{\gamma_4}{6}\sum_{\vec{G}'}\sum_{\vec{G}''} A_{\vec{G}'}A_{\vec{G}''}A_{\vec{G}-\vec{G}'-\vec{G}''}\right\} + \eta_{\vec{G}}(t). \tag{18}$$

This is the same equation as equation (15), except that now $\{A_{\vec{G}}\}$ includes both the order parameter of the original structure and the dominant fluctuation modes.

Note that, in this representation, the locations of the fluctuation modes are consistent with the result of anisotropic fluctuation. For example, fluctuations on the lamellar phase with a wavevector $\vec{G}_1$ are captured by the wavevectors $\vec{G}_2$, $\vec{G}_3$, $\vec{G}_5$, $\vec{G}_6$, which reside on the ring identified in *Figure 2*. The fact that here we have a discrete mode of fluctuation, instead of the continuum of modes on the ring from the previous analysis, is of little consequence at the linear order of the fluctuation. For example, the same spinodal is predicted independent of the number of modes used. (This is generally true in any linear stability analysis.) Thus, the simplified mode analysis is consistent with the full analysis in Section 2 and Section 3.1 at the level of linear stability analysis, but has the advantage of allowing a simple qualitative description of the system in the nonlinear regime.

In *Figure 11* we show the temporal evolution of the various modes for the LAM to HEX transition after a sudden temperature jump, obtained by a direct numerical integration of equation (18). (For simplicity, we included the random noise term in the initial conditions for the various modes, but did not keep it during the simulation; this turned out not to have qualitative effects on the dynamical behaviours.) The kinetic path starts with a rapid decrease of the lamellar order parameter which then quickly turns to a plateau. During this initial phase, the amplitudes of the other modes remain small. Thus the system remains in a lamellar state. At the end of the first plateau, the other modes (which in the case of LAM represent the anisotropic fluctuations) begin to grow and at the same time the amplitude of the lamellar wave undergoes another drop. The system then reaches another plateau. On this plateau, the amplitudes $A_{\vec{G}_2}$ ($= A_{\vec{G}_3}$) and $A_{\vec{G}_5}$ ($= A_{\vec{G}_6}$) are degenerate; they bifurcate towards the end of this plateau when $A_{\vec{G}_2}$ merges with the lamellar wave $A_{\vec{G}_1}$ while $A_{\vec{G}_5}$ and $A_{\vec{G}_4}$ decrease to zero to form the hexagonal cylinder structure. This stagewise behaviour is consistent with the full simulation results (*Figure 5*). (The durations of the plateau are subject to the specific realization of the noise terms and hence are not particularly meaningful.) Evolution of the microstructure is well captured by superposing the various modes. In particular, taking the order parameters in the transition region between the first and second plateaus, and in the middle of the second plateau, respectively, we reproduce the two intermediate states, the modulated lamellar and perforated lamellar structures, observed in *Figure 6b* and *Figure 6c*.

In *Figure 12*, we show a phase portrait in terms of $A_{\vec{G}_1}$ ($= A_{\vec{G}_2} = A_{\vec{G}_3}$) and $A_{\vec{G}_5}$ ($= A_{\vec{G}_4} = A_{\vec{G}_6}$) for the HEX to DIS transition in the case of a shallow temperature jump. The transient growth of $A_{\vec{G}_5}$ is the result of the instability discussed in Section 3.1. While the linear analysis there predicted that the fluctuation modes (which are part of a BCC or twinning BCC lattice) would grow at some point along the kinetic path, the nonlinear analysis presented here allows us to predict the full trajectory of the system. *Figure 12* depicts the full pathway of the system starting from a HEX structure, going through a transient BCC-modulated hexagonal state, and eventually melting to the DIS state.

Using the extended set of order parameters, one can construct a simple free energy function. The free energy landscape in this order parameter space offers some

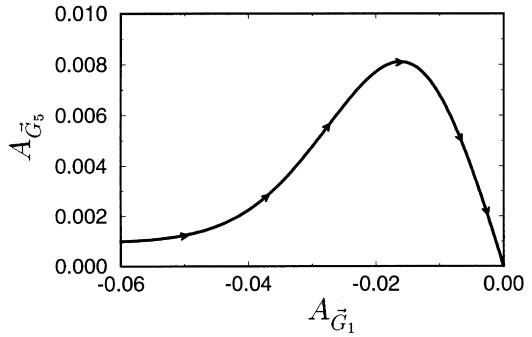

Figure 12 Phase portrait for the HEX to DIS transition for a temperature jump from $(N\chi)_i = 11.71$ to $(N\chi)_f = 11.20$ at $f = 0.4$. The nonzero initial $A_{\vec{G}_5}$ is due to the initial perturbation

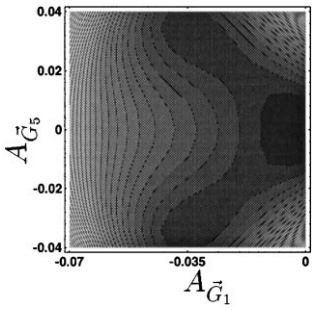

Figure 13 The ridgelike structure of the free energy surface for $(N\chi)_f = 11.20$ and $f = 0.4$

additional insight into the nature of the kinetic pathways. For example, the two plateaus in *Figure 11* for the LAM to HEX transition are seen to correspond to two saddle points in the free energy surface. The first plateau is near the point where the fluctuations around the lamellar structure become unstable. These fluctuations (captured in the current analysis by $A_{\vec{G}_2}$ and $A_{\vec{G}_5}$) lead to correlated lateral modulations in the lamellar structure which grow into a perforated lamellar (PL) structure. The second plateau corresponds to such a PL structure which is itself another saddle point; the most unstable direction being the bifurcation between $A_{\vec{G}_2}$ and $A_{\vec{G}_5}$ which leads to the final HEX structure. The nature of the PL structure has been discussed in our recent publication[17].

In the case of the HEX to DIS transition, a study of the free energy shows that the landscape (in the parameter space of $A_{\vec{G}_1}$ and $A_{\vec{G}_5}$) has two qualitatively different appearances depending on the extent of the temperature jump. For $(N\chi)_f = 10.97$ corresponding to the larger temperature jump, the free energy surface is parabolic with a simple minimum at $A_{\vec{G}_1} = 0$ and $A_{\vec{G}_5} = 0$. However, for $(N\chi)_f = 11.20$, the free energy surface has a ridgelike feature as shown in *Figure 13*. The transient appearance of the BCC-modulation during the melting of the hexagonal cylinders is thus a result of deflection from the direct downhill path, $A_{\vec{G}_5} = 0$.

Though we have discussed only the LAM to HEX and HEX to DIS transitions explicitly, the analyses (in both Section 3.1 and Section 3.2) can be applied to studying other transitions as well.

4. DISCUSSION

In this paper, we have described a unified approach to understanding the various order–order and order–disorder transitions in weakly ordered diblock copolymers. Our theory is based on the concept of anisotropic fluctuations of the order parameter in the ordered structures. The emergence of new structures, whether they are the final equilibrium structures, or transient structures on the kinetic pathways, is due to the growth of the most unstable fluctuation modes. A systematic linear stability analysis is presented both for the equilibrium states—in order to locate the spinodal of the initial structure and identify the least stable fluctuation modes—and for nonequilibrium states where the thermodynamic driving force is nonvanishing. In the latter case, it is shown that the thermodynamic driving force can be separated into a meanfield, deterministic contribution that governs the evolution of the meanfield order parameter associated with the initial structure, and a fluctuating contribution that determines the stability of the meanfield path and is responsible for the emergence of new structures. The linear stability analysis allows us to determine the stability of the meanfield path for any given value of the meanfield order parameter of the kinetic path. By combining the largest fluctuation modes and the order parameter of the initial structure into an expanded order parameter space, we are able to describe qualitatively the full nonlinear evolution of the system during the various transitions.

In recent years, there have been a number of experiments aimed at probing various dynamical aspects of the order–order and order–disorder transitions in block copolymers[18–27]. However, experiments that directly address the kinetic pathways after temperature jumps are few and are perhaps difficult. Nevertheless, some tentative comparisons can be made between theory and experiments where such comparisons are appropriate.

We start with the shear cessation experiments of Bates and co-workers[25]. In one of these experiments, an initially disordered phase of asymmetric poly(ethylenepropylene)–poly(ethylethylene) (PEP–PEE) diblock copolymer close to the order–disorder boundary is subjected to a constant shear which induces a transition to the HEX phase (with the cylinders aligned along the shear direction). The shear is suddenly stopped, and the system is now in a condition favouring the DIS phase. These authors observed that the cylinders first break into spheres before melting to the DIS phase, much akin to what we find after a temperature jump. Insofar as a HEX phase is created and then the condition is changed to favouring the DIS phase, the shear-cessation experiment can be likened to a temperature jump experiment. We believe the mechanism described in this paper is responsible for their observations.

The HEX to BCC transition has also been studied by Bates and co-workers[24]. These authors showed that BCC spheres pinch off from the HEX cylinders such that the cylinder's axis is the (111) direction of the resulting BCC structure which they term the 'epitaxial' relationship. They also suggested that the BCC phase forms by way of an undulating cylinder structure. These are in agreement with our mechanism[4,5].

Thermally induced LAM to HEX transition has been studied by Hajduk *et al.*[23] for the poly(styrene–*b*-ethene-co-butene) diblock copolymer. However, these authors did not observe the appearance of the intermediate modulated/perforated lamellar structure predicted by our theory and simulation (see *Figure 6*). We have shown earlier[5] that a distinct intermediate PL structure appears only in a certain temperature window in the LAM to HEX transition; see Fig. 15 of Ref. [5]. It is possible that the temperature jump in

the experiment is too large for a distinct intermediate PL to appear, but further studies are needed to fully resolve the discrepancy between theory and experiment.

On the other hand, the perforated lamellar (PL) structures have been observed in several experiments by Bates' group[28–30] in regions of the phase diagram between the LAM and HEX or the G phase. In a very recent paper by Hajduk *et al.*[31], an extensive series of new experiments demonstrate quite convincingly that the PL is a kinetic state en route from the LAM phase to the HEX or the G phase, thus providing indirect evidence of our proposed LAM to HEX transition mechanism. Although further studies are required, we found, both through direct computer simulation, and through theoretical analysis, that the PL state during the transition from LAM to HEX after a temperature jump can be made metastable by a sudden temperature quench back to the initial temperature: instead of going back to the LAM phase, the system gets trapped in a metastable PL state. It is possible that the PL structures reported by Bates and co-workers, that had been initially thought to be equilibrium phases, were in fact kinetically trapped states due to a combination of thermal and shear operations used in the experiments.

As concluding remarks, we mention two outstanding issues related to fluctuations in ordered block copolymer phases and kinetics of order–order and order–disorder transitions. The first issue concerns the renormalization effects due to nonlinear fluctuations on the stability of the ordered phases. The Brazovskii–Fredrickson–Helfand theory[32,33] assumes isotropic fluctuations and treats these fluctuations by a simple Hartree approximation. Although capable of capturing several new qualitative features, including the prediction that the DIS to LAM transition becomes first order, the theory cannot be an accurate description of the ordered phases. It is thus of interest to study the effects of nonlinear anisotropic fluctuations. The anisotropic fluctuation effects will be most pronounced for asymmetric compositions due to the renormalization from the γ_3-term, which is absent in the isotropic Hartree theory. In addition to shifts in the phase boundaries, an interesting issue is whether the spinodals of the ordered phases predicted from the linear theories (the theory in this work and that in Refs [6,7]) can survive the renormalization.

Another issue concerns the effects of shear flow. Experimentally it is much more convenient to cross phase boundaries by applying a flow field than by changing the temperature. Changes in the small-angle neutron scattering patterns of ordered block copolymer phases due to shear have been demonstrated in several experiments by the Bates' group[28–30]. These results reflect the distortion of the spectrum of anisotropic fluctuations. However, no theory is currently available. We plan to address the effects of shear flow on anisotropic fluctuations and the various spinodals, first by a linear theory and then by a renormalized theory that accounts for the nonlinear, anisotropic fluctuations.

ACKNOWLEDGEMENTS

This research is supported in part by the National Science Foundation (Grant Nos. ASC-9217368 and DMR-9531914), the Camille and Henry Dreyfus Foundation (Award No. TC-96-063) and the Alfred P. Sloan Foundation (Award No. BR-3508).

REFERENCES

1. Gunton, J. D., Miguel, M. S. and Sahni, P. S., in *Phase Transition and Critical Phenomena*, Vol. 8, ed. C. Domb and J. L. Lebowitz. Academic Press, New York, 1983.
2. Bates, F. S., *Science*, 1991, **251**, 898, Bates, F. S. and Fredrickson, G. H., *Ann. Rev. Phys. Chem.*, 1990, **41**, 525; Fredrickson, G. H. and Bates, F. S., *Ann. Rev. Mater. Sci.*, 1996, **26**, 501.
3. Matsen, M.W. and Schick, M., *Curr. Op. Coll. Interface Sci.*, 1996, **1**, 329.
4. Qi, S.Y. and Wang, Z.-G., *Phys. Rev. Lett.*, 1996, **76**, 1679.
5. Qi, S.Y. and Wang, Z.-G., *Phys. Rev. E.*, 1997, **55**, 1682.
6. Laradji, M., Shi, A.-C., Desai, R. C. and Noolandi, J., *Phys. Rev. Lett.*, 1997, **78**, 2577; *Macromolecules*, in press.
7. Yeung, C., Shi, A.-C., Noolandi, J. and Desai, R. C., *Macromol. Theory Simul.*, 1996, **5**, 291; Shi, A.-C., Noolandi, J. and Desai, R. C., *Macromolecules*, 1996, **29**, 6487.
8. Leibler, L., *Macromolecules*, 1980, **13**, 1602.
9. Ohta, T. and Kawasaki, K., *Macromolecules*, 1986, **19**, 2621.
10. Almdal, K., Koppi, K.A. and Bates, F.S., *Macromolecules*, 1993, **26**, 4058.
11. de Gennes, P.G., *J. Chem. Phys.*, 1980, **72**, 4756.
12. Pincus, P., *J. Chem. Phys.*, 1981, **76**, 1996.
13. Binder, K., *J. Chem. Phys.*, 1983, **79**, 6387.
14. Fredrickson, G.H., *J. Chem. Phys.*, 1986, **85**, 5306.
15. Kawasaki, K. and Sekimoto, K., *Physica*, 1988, **143A**, 349; *Physica* 1988, **148A**, 361.
16. Kumaran, V. and Fredrickson, G.H., *Physica*, 1994, **204A**, 378.
17. Qi, S.Y. and Wang, Z.-G., *Macromolecules*, 1997, **30**, 4491.
18. Hashimoto, T., Kowsaka, K., Shibayama, M. and Suehiro, S., *Macromolecules*, 1986, **19**, 750; Hashimoto, T., Kowsaka, K., Shibayama, M. and Kawai, H., *Macromolecules*, 1986, **19**, 754.
19. Singh, M. A., Harkless, C. R., Nagler, S. E., Shannon, R. F. and Ghosh, S. S., *Phys. Rev. B*, 1993, **47**, 8425; Harkless, C. R., Singh, M. A., Nagler, S. E., Stepheson, G. B. and Jordan-Sweet, J. L., *Phys. Rev. Lett.*, 1990, **64**, 2285.
20. Sakurai, S., Momii, T., Taie, K., Shibayama, M., Nomura, S. and Hashimoto, T., *Macromolecules*, 1993, **26**, 485.
21. Sakurai, S., Kawada, K., Hashimoto, T. and Fetters, L.J., *Macromolecules*, 1993, **26**, 5796.
22. Floudas, G., Hadjichristidis, N., Iratrou, H., Pakula, T. and Fischer, E. W., *Macromolecules*, 1994, **27**, 7735; Floudas, G., Vlassopoulos, D., Pitsikalis, M., Hadjichristidis, N. and Stamm, M., *J. Chem. Phys.*, 1996, **104**, 2083; Floudas, G., Hadjichristidis, N., Stamm, M., Likhtman, A. E. and Semenov, A. N., *J. Chem. Phys.*, 1997, **106**, 3318.
23. Hajduk, D.A., Gruner, S.M., Rangarajan, P., Register, R.A., Fetters, L.J., Honeker, C., Al-balak, R.J. and Thomas, E.L., *Macromolecules*, 1994, **27**, 490.
24. Schulz, M. F., Bates, F. S., Almdal, K., Mortensen, K., *Phys. Rev. Lett.*, 1994, **73**, 86; Koppi, K. A., Tirrell, M., Bates, F. S., Almdal, K. and Mortensen, K., *J. Rheol.*, 1994, **38**, 999.
25. Koppi, K. A., Ph.D. Thesis, The University of Minnesota, 1994; Bates, F. S., Koppi, K. A. and Tirrell, M., *Macromolecules*, 1994, **27**, 5934; Almdal, K., Mortensen, K., Koppi, K. A., Tirrell, M. and Bates, F. S., *J. Phys. II*, 1996, **6**, 617.
26. Dai, H.J., Balsara, N.P., Garetz, B.A. and Newstein, M.C., *Phys. Rev. Lett.*, 1996, **77**, 3677.
27. Ryu, C. Y., Lee, M. S., Hajduk, D. A. and Lodge, T. P., *J. Poly. Sci. Poly. Phys. Ed.*, 1997, **35**, 2811.
28. Hamley, I.W., Koppi, K.A., Rosedale, J.H., Bates, F.S., Almdal, K. and Mortensen, K., *Macromolecules*, 1993, **26**, 5959.
29. Förster, S., Khandpur, A.K., Zhao, J., Bates, F.S., Hamley, I.W., Ryan, A.J. and Bras, W., *Macromolecules*, 1994, **27**, 6922.
30. Khandpur, A.K., Förster, S., Bates, F.S., Hamley, I.W., Ryan, A.J., Bras, W., Almdal, K. and Mortensen, K., *Macromolecules*, 1995, **28**, 8796.
31. Hajduk, D. A., Takenouchi, H., Hillmyer, M. A., Bates, F. S., Vigild, M. E. and Almdal, K., *Macromolecules*, 1997, **30**, 3788.
32. Brazovskii, S.A., *Sov. Phys. JEPT*, 1975, **41**, 85.
33. Fredrickson, G.H. and Helfand, E., *J. Chem. Phys.*, 1987, **87**, 697.